Evolving spin periodicity and lock-in transition in the frustrated ordered ilmenite-type β-Mn 2 InSbO 6

Ángel M Arévalo-López, Elena Solana-Madruga, Eugenia P Arévalo-López, Dmitry Khalyavin, Michal Kepa, Antonio J dos Santos-García, Regino Sáez-Puche, J. Paul Attfield

Evolving spin periodicity and lock-in transition in the frustrated ordered ilmenite-type β-Mn_2InSbO_6.

Ángel M. Arévalo-López[1], Elena Solana-Madruga[2], Eugenia P. Arévalo-López[3], Dmitry Khalyavin[4], Michal Kepa[2], Antonio J. Dos santos-García[5], Regino Sáez-Puche[6] and J. Paul Attfield[2]

[1] Univ. Lille, CNRS, Centrale Lille, ENSCL, Univ. Artois, UMR 8181 - UCCS, F-59000 Lille, France.
[2] Centre for Science at Extreme Conditions and School of Chemistry, University of Edinburgh, EH9 3FD, U.K.
[3] Física Atómica y Molecular, Facultad de Ciencias, UNAM. Ciudad Universitaria, 58000, México.
[4] ISIS Facility, Rutherford Appleton Laboratory Harwell Oxford, Didcot OX11 0QX, U.K.
[5] Dpto. Ingeniería mecánica, Química y Diseño Industrial, ETSIDI, UPM, 28012 Madrid, Spain.
[6] Dpto. Química Inorgánica, Fac. Químicas, Universidad Complutense de Madrid, 28040 Madrid, Spain.

Polar magnets are promising materials for new applications as multiferroics or in spintronics. In double corundum-related oxides, the cation ordering imposes a polar structure and the use of high pressure facilitates the insertion of magnetic cations into the compounds. Here we present the high-pressure synthesis of a new polar and ferrimagnetic corundum derivative Mn_2InSbO_6, which adopts the ordered-ilmenite-type structure. Neutron powder diffraction reveals that the high-temperature nearly collinear ferrimagnetic phase evolves to an incommensurate helical structure with $k_\delta = [0\ 0\ k_z]$ propagation vector, which then locks to the commensurate value of $k_z = 1/8$. This complex magnetic behavior is likely to be related to magnetic frustration and the polar nature of the ordered double corundum structure.

I. INTRODUCTION

High pressure and high temperature treatments of ABO_3 oxides promote unusual cationic arrangements and interesting physical properties.[1] For instance, at ambient pressure, both $MnXO_3$ with X = V and Ti crystallise in the ilmenite-type structure. They consist in hexagonal closed-packed oxygens with two-thirds of the octahedral holes filled with Mn and V or Ti in an ordered-layer fashion along the z-direction with a non-polar *R-3* space group. Under high pressure conditions, $MnVO_3$-II shows a perovskite structure with itinerant $3d^1$ V^{4+} and localised $3d^5$ Mn^{2+} electrons, where the spins order in a helical magnetic structure.[2] $MnTiO_3$-II presents a $LiNbO_3$-type, where the cations order along the [111] direction of the cubic cell with the polar *R3* space group. It presents multiferroic properties due to Dzyaloshinskii-Moriya exchange interactions (DM).[3] Following explorations of the double perovskites family, with more than 600 members,[4] double corundum derivatives $A_2BB'O_6$ have demonstrated their potential for new multifunctional materials with magnetic ions into both A- and B-sites of Ni_3TeO_6- and ordered-ilmenite structural types with *R3* polar space group.[5] However, despite the possible combinations, only 15 polar $A_2BB'O_6$ double corundum-related compounds have been reported to date. Of these, three are theoretical predictions [6, 7], four synthesised at ambient pressures [8, 9, 10] and the rest can only be stabilised under high pressure and temperature conditions [11, 12, 13,14, 15, 16, 17, 18, 19] (Supplementary Table S2).

The polar lattice of double corundum-type oxides can also stimulate the formation of modulated spin structures via a mechanism described by Lifshitz invariants in a Landau free- energy expansion.[20,21] This gradient energy term favour inhomogeneous magnetic states and is known to result in incommensurate magnetic ground states in MnSi [22] and $BiFeO_3$ [23, 24]. Both of these compounds demonstrate rich phase diagrams including magnetic field induced skyrmion lattice [25] and high-temperature multiferroic properties respectively[26].

In this work, we present the high pressure synthesis of a new polar and magnetic double corundum oxide Mn_2InSbO_6. The compound has been found to exhibit a remarkable evolution between complex magnetic structures towards a long-period modulated ground state compatible with the mechanism promoted by the gradient Lifshitz terms.

II. EXPERIMENTAL

Mn_2InSbO_6 sample was synthesised under high pressure-high temperature conditions. The stoichiometric proportions of Mn_2O_3, In_2O_3 and Sb_2O_3 oxides were ground under acetone to prepare the precursor mixture and treated at 5 GPa and 1373 K during 20 minutes using a Walker-type multianvil apparatus. After the reaction time, the temperature was quenched and the pressure was slowly released. High resolution powder XRD data were collected for Mn_2InSbO_6 at 80 K, 40 K, 30 K, 20 K, 17 K, 14 K,

10 K, 8 K, 6 K and 4 K in the 5 º < 2θ < 40 º angular range with a 0.03º step size using λ = 0.467173 Å synchrotron radiation at the BL04-MSPD beamline at ALBA light source (Barcelona, Spain). For the refinement of the SXRD data, the background was modelled with a list of experimental equidistant points afterwards refined through the linear interpolation of intermediate values and the peak shape was fitted using a Thompson-Cox-Hastings type function. Neutron powder diffraction (NPD) profiles were collected for Mn_2InSbO_6 at 2 K, 4 K, 6 K, 8 K, 10 K, 14 K, 17 K, 20 K, 30 K, 40 K and 80 K using the WISH instrument (ISIS facility, Oxford, U.K). The crystal and magnetic structures were refined using the FullProf suite [27]. The nuclear scattering was modeled in the *R3* space group and the magnetic intensities were introduced in the refinement procedure using the propagation vectors formalism with k_1= [0 0 0] (20 K), k_2 = [0 0 1/8] (2 K) and k_δ = [0 0 k_z] (intermediate temperatures). Magnetic symmetry analysis was carried out using the program BasIreps [27] for *R3* space group. Magnetic susceptibility measurements were performed on a Quantum Design XL-MPMS SQUID magnetometer under DC Zero-Field-Cooling (ZFC) and Field-Cooling (FC) conditions in the temperature range 2 K < T < 100 K under magnetic fields of 0.5 T and 0.01 T. Magnetization hysteresis loops were measured at 2 K, 10 K, 17 K, 20 K, 40 K and 60 K up to 3 T. Specific heat was measured using a Quantum Design PPMS under magnetic fields of 0 T, 3.5 T and 7 T. The dielectric response was measured on cooling with a Andeen-Hagerling Capacitance bridge at 1 kHz in a closed cycle refrigerator.

III. RESULTS AND DISCUSSION

A. Crystal Structure

Mn_2InSbO_6 prepared at ambient pressure crystallises in the Mg_3TeO_6-type structure, another corundum type derivative with *R-3* centrosymmetric group (*a* = 8.93 Å and *c* = 10.71 Å) and all cations in octahedral coordination but with manganese and indium fully disordered.[28] The polycrystalline β-Mn_2InSbO_6 polymorph reported here requires high-pressure synthesis at 5 GPa and 1373 K (see Experimental Section). Initial laboratory X-ray diffraction indicated a rhombohedral cell (*a* ≈ 5.38 Å, *c* ≈ 14.21 Å) and a small amount of unreacted In_2O_3 (<5 % wt). Rietveld analysis of combined high-resolution synchrotron X-ray (SXRD) and neutron powder (NPD) diffraction

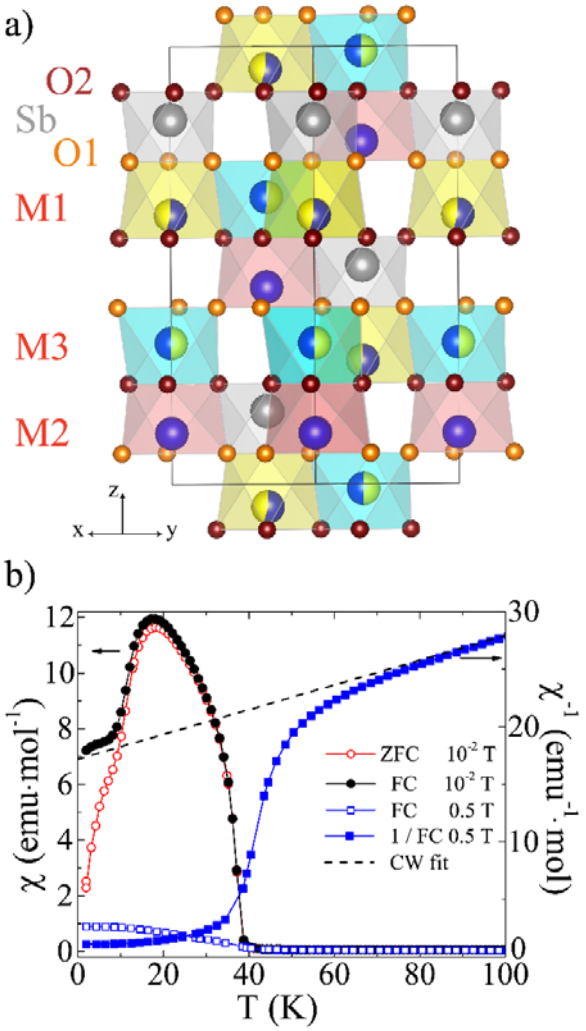

Figure 1. a) Crystal structure of $(Mn_{0.5}In_{0.5})_2MnSbO_6$ along [110] direction. Grey and blue spheres represent the ordered Sb and Mn sites respectively. Blue-yellow spheres show the mixed Mn-In sites. b) Thermal evolution of the direct and inverse magnetic susceptibilities measured at 0.5 and 0.01 T in FC and ZFC modes. Dashed line represents the Curie-Weiss fit.

data collected at 80 K (Supplementary Fig. S1) revealed that Mn_2InSbO_6 crystallises in a double-corundum-type derivative. It presents alternating *xy* honeycomb layers formed by ordered Sb / Mn and disordered In / Mn octahedra sharing edges, stacked along the *z* axis. This structure is known as Ordered-Ilmenite-type (OIL-type).[29] The contrast between Mn, In and Sb arising from their neutron scattering lengths (Mn = -3.73 fm, In = 4.06 fm, Sb = 5.57 fm) and X-ray form factors (Z = 25, 49, 51) allowed their antisite disorder to be quantified from combined NPD and SXRD refinement. One cation layer is fully ordered with Sb and Mn (site *M*2) and one is fully

disordered between Mn and In (*M*1 and *M*3). The crystal structure is shown in Figure 1a and the final refinement results at 80 K are listed in Supplementary Table S3.

The antisite exchange between *M*1 and *M*3 within the layer results in a larger Mn occupancy at both *M*1 (51.2 %) and *M*3 (55.5 %) sites in good agreement with the In deficiency matching the minor In_2O_3 secondary phase. For *M*2 and Sb sites, refinements suggested no disorder (antisite allowance refined to <1% with no fit improvement), so hereafter we will refer to the compound as $(Mn_{0.5}In_{0.5})_2MnSbO_6$. This selective site exchange reflects the small size and charge mismatch between In^{3+} (r^{VI} = 0.8 Å) and Mn^{2+} (r^{VI} = 0.83 Å) compared to that between Sb^{5+} (r^{VI} = 0.6 Å)[30] and Mn^{2+}. Bond valence sums (BVS) calculations with an interpolation method[31] result in +2.34, +2.39, +2.09, +5.10, for *M*1, *M*3, *M*2 and Sb in agreement with formal cationic oxidation states and anti-site disorder of $(Mn_{0.5}^{2+}In_{0.5}^{3+})_2Mn^{2+}Sb^{5+}O_6$. The proposed formal cation oxidation states are supported by X-ray photoelectron spectroscopy (XPS) measurements (Supplementary Table S1 and Fig. S4) [32, 33, 34, 35, 36, 37]. Bond distances and angles are registered in Supplementary Table S8.

B. Magnetic Properties and Magnetic Structure

The combination of magnetic cations in *M*1, *M*2 and *M*3 sites and anti-site disorder for *M*1 and *M*3 gives rise to a complex magnetic behavior. Temperature dependent magnetisation measurements for $(Mn_{0.5}In_{0.5})_2MnSbO_6$ in 0.01 T and 0.5 T fields (Fig. 1b) show a ferrimagnetic transition at T_{N1} = 38(1) K and Curie-Weiss paramagnetism at higher temperatures with a paramagnetic moment of 6.1(1) μ_B / Mn, close to the theoretical value of 5.92 μ_B for localised S = 5/2 Mn^{2+}, and a Weiss temperature of θ = –160(1) K showing that antiferromagnetic spin-spin interactions are dominant but partially frustrated ($|\theta| / T_N \approx 4$). A further transition is evidenced in the 0.01 T magnetic susceptibility curves at T_{N2} = 8(1) K, where zero field and field cooled data diverge from each other. Magnetic hysteresis loops and heat capacity measurements show also transitions at T_{N1} and T_{N2}, see Supporting Information.

NPD data were analysed to understand the low-temperature magnetic behavior in $(Mn_{0.5}In_{0.5})_2MnSbO_6$. On cooling below T_{N1} = 38 K, magnetic diffraction intensity is observed, for instance on (003) and (101) peaks at ~ 4.7 Å and ~ 4.4 Å as shown in Figure 2a. All the magnetic diffraction peaks observed down to 17 K can be indexed with propagation vector k_1 = [0 0 0]. Below T_δ = 17 K the intensity of the magnetic diffraction peaks decreases and new satellite peaks appear. Their position gradually changes, revealing a second transition with k_δ = [0 0 k_z] that locks-in at a third transition with k_z = 1/8 at T_{N2} = 8 K. The thermal evolution of k_z is shown on the right panel of Figure 2a. k_z increases from 0 to 1/8 on cooling and it evidences the gradual commensurate to commensurate (k_1 to k_2) magnetic transition through a continuum of helical magnetic structures. Rietveld fits of both commensurate magnetic structures are shown on difference patterns of 20 K – 40 K (k_1) and 2 K – 40 K (k_1 + k_2) in Figure 2b left and the crystallographic details are summarised in Tables S4 and S5. Symmetry analysis allows a consistent description of the different magnetic structures. For stable refinements, the magnetic moment per Mn ion in the three different Mn sites were constrained to be the same. In the k_1 = [0 0 0] phase, the strongest magnetic interactions are the direct (AFM) M-M interactions between cations

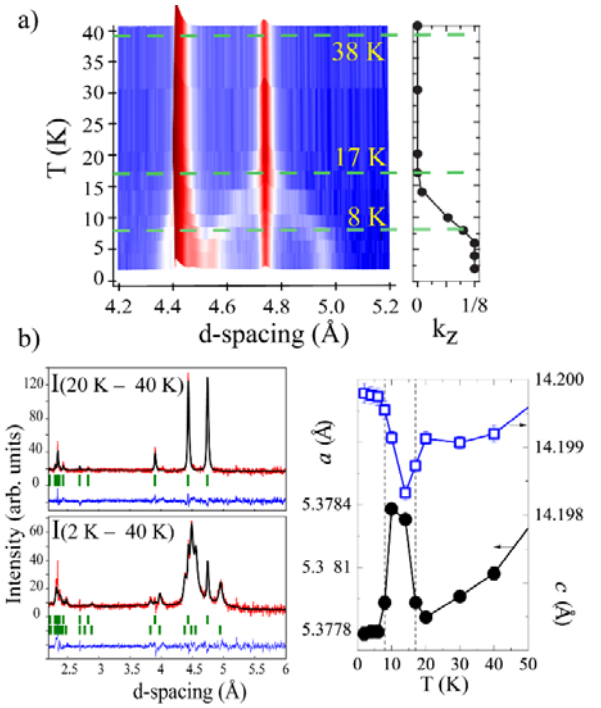

Figure 2. a) 2D contour plot showing the temperature evolution of the (003) and (101) magnetic diffraction maxima. The green lines at 38 K, 17 K and 8 K mark the transitions between the different magnetic structures. The panel on the right shows the change on the *z* component of the propagation vector k_δ = [0 0 k_z]. b) Magnetic structure fits to the difference between 20 K and 40 K (top) and 2 K and 40 K (bottom) WISH NPD profiles of $(Mn_{0.5}In_{0.5})_2MnSbO_6$. The vertical ticks indicate the positions of the Bragg reflections for k_1 = [0 0 0] (20 K) and k_2 = [0 0 1/8] (2 K) (lower row) models. The panel on the right shows the thermal evolution of the cell parameters, revealing magnetostriction induced by the evolving magnetic structure.

located into face-sharing octahedra, i.e. M2-M3 (d ~ 2.9 Å). Therefore, ferromagnetic layers *M*1/*M*3 and *M*2 stack antiferromagnetically with the spins ordered

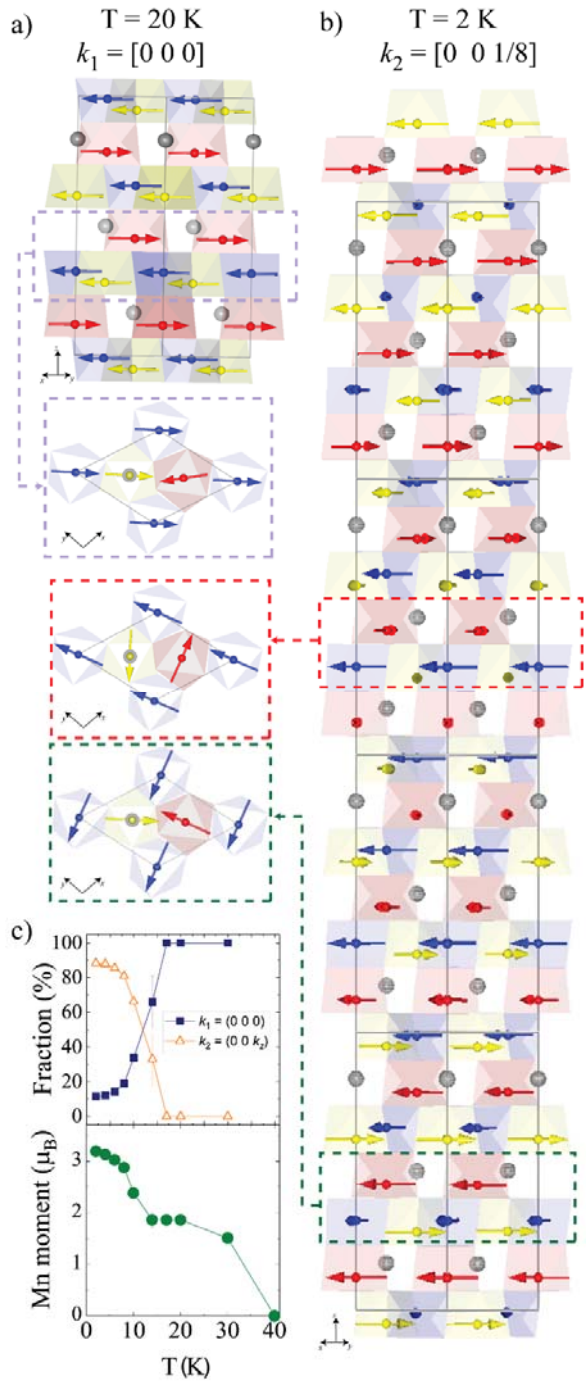

Figure 3. [001] and [110] projections of the magnetic structures of $(Mn_{0.5}In_{0.5})_2MnSbO_6$. Yellow, red and blue arrows represent the Mn^{2+} spins at *M*1, *M*2 and *M*3 sites respectively (Y, R, B). a) k_1 = [0 0 0] at 20 K. b) Half-cell of the k_2 = [0 0 1/8] structure showing the frustration relieved by B rotation; there is a 15º rotation between Y-R-B spins slabs. c) Thermal evolution of the magnetic moments and phase fraction. It reveals the progressive transition of the k_1 model into the k_2 model below 17 K, both coexisting at 2 K.

along the [110] direction with a refined magnetic moment of 1.9(1) μ_B / Mn^{2+} at 20 K (Figure 3a). Antisymmetric DM exchange interactions are allowed in the non-centrosymmetric space group *R3*. The spontaneous ferromagnetic component in this phase, observed in magnetisation measurements, probably comes from the uncompensated magnetization of the sublattices (ferrimagnetic) and canting of the spins (weak-ferromagnetism). Single crystal analysis will be needed to refine the ordered moments of the three magnetic sublattices independently. However, the d^5-d^5 interactions within the (00l) layers via superexchange through oxygen at ~ 90 º should be AFM according to Goodenough-Kanamori-Anderson rules. Below T_δ = 17 K, the interactions between the magnetically diluted M1/M3 sites strengthens and their honeycomb arrangement originates a strong magnetic frustration. This effect induces another transition, mainly in the M3 (blue) site, with a partial relief of frustration leading to spin reorientation as shown in Figure 3b. All previously reported Mn_2BSbO_6 corundum derivatives have only two independent magnetic sites, originating the rigid rotation of the FM layers. The OIL structure of Mn_2InSbO_6 has three independent magnetic sites, what increases the degrees of freedom and allows for the independent rotation of the spins within the honeycomb layers.

Below T_{N2} = 8 K the magnetic structure locks-in into a commensurate state with k_2 = [0 0 1/8], in accordance with the magnetisation and heat capacity measurements (Supporting Information). The structure describes *M*1 – *M*2 – *M*3 layers of spins with a relative orientation of 0º ~ 170º ~ 120º between their spin directions and with a 15º rotation between slabs (Figure 3b). The refined magnetic moment of 3.2(1) μ_B per Mn at 2 K is significantly lower than the ideal value of 5 μ_B for S= 5/2 Mn^{2+} showing that frustration is still present. Magnetic diffuse scattering is present at 2 K, see Figure S3 in SI. The two magnetic structures coexist below 17 K and 11% of the k_1 phase persists at 2 K. Combined Rietveld refinements of SXRD and NPD patterns collected between 2 K and 40 K (Table S7) reveal magnetostriction in the cell parameters when the spin reorientation takes place, Figure 2b right.

C. Dielectric properties

The OIL-type structure of $(Mn_{0.5}In_{0.5})_2MnSbO_6$ with polar *R3* space group is expected to present a net spontaneous polarisation. However, no switching is possible since the loss of centre of symmetry comes from cation ordering and not from cooperative ion

motion (i.e. the material is an improper ferroelectric). The variation of the permittivity and the dielectric loss (tan δ) thermal responses show an increase below T_δ = 17 K, Fig. 4 (top). These variations resemble the magnetostriction observed in the cell parameters as shown in Figure 2b. The observed magnetostriction is coupled to the additional displacements of the cations along the *c* axis below T_N. This ionic motion is expected to originate an increase of the polarization (P_s). The expected P_s has been estimated using a point charge model from the experimental atomic displacements. When compared to the predicted value at 80 K (~ 12 μC / cm^2), P_s shows a negligible change at 40 K, but it gradually increases below T_{N1} up to ~25% of ΔP_s (~ 15 μC / cm^2) when it adopts an incommensurable magnetic structure at 14 K. This polarisation is directly related to the expansion (contraction) of *M*2 and Sb (*M*1 and *M*3) octahedra, as shown at the bottom of Figure 4, induced by the magnetic order. The octahedral distortion has been calculated in terms of their mean ellipsoid radii (<R>) and shape (S) parameters from Pieface software [38]. The results, shown in Fig. S6, confirm the described cooperative evolution of the octahedral distortions resulting from the magnetic transition at T_{N1}.

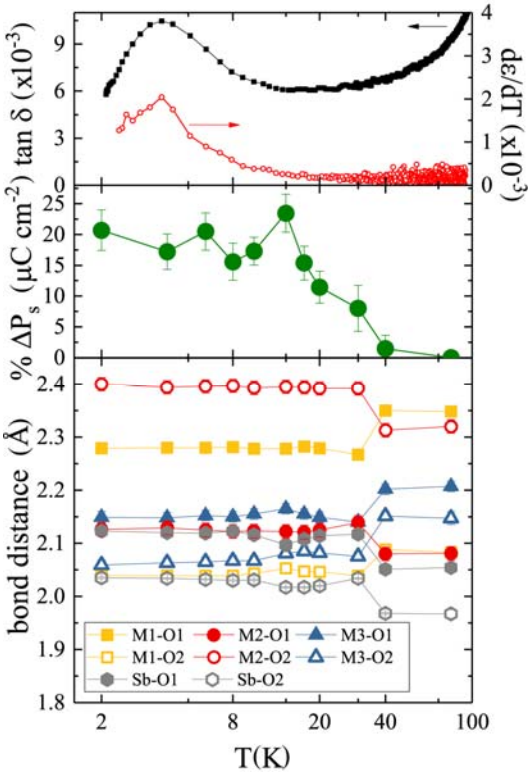

Figure 4. Thermal evolution of the dielectric response of $(Mn_{0.5}In_{0.5})_2MnSbO_6$ (top) showing a transition in the dielectric permittivity below 8 K. The variation in the polarization (middle), determined from the experimental atomic displacements using point-charge model calculations, evidence the onset of a weak magnetoelectric coupling at T_{N1} = 38 K which becomes progressively stronger upon cooling down to T_{N2} = 8 K. Thermal behaviour of average <M-O> bonds (bottom).

D. Relevant Free-Energy terms

The non-collinear orientation of the three magnetic sublattices in the helical phase (Figure 3b) strongly points to the presence of competing exchange interactions in the system. The inter-sublattice interactions are antiferromagnetic and comparable in magnitude, giving rise to magnetic frustration. Another important mechanism promoting incommensurate spin ordering is related to the polar nature of the crystal structure of Mn_2InSbO_6. This implies that the physically irreducible representation GM2GM3(η,η^*) which transforms the magnetic order parameter in the high-temperature $\boldsymbol{k}$=0 phase, allows the presence of gradient Lifshitz invariant in the Landau free-energy decomposition, $\eta\frac{\partial\eta^*}{\partial z}-\eta^*\frac{\partial\eta}{\partial z}$. The component of the gradient operator is transformed by the totally symmetric representation and the transformational properties of the magnetic order parameter are specified in Table S9 and S10 of the Supplemental information. This term favours an inhomogeneous magnetic state [39,40] propagating along the Λ-line of symmetry ($\boldsymbol{k}$ = 0,0,k_z) and is expected to have a strong impact on the magnetic ground state in systems without strong single ion anisotropy. The mechanism involves relatively weak anti-symmetric DM exchange interactions at a microscopic level. The latter usually implies a long-period modulation. A nearly quenched orbital angular momentum expected for Mn^{2+} cations and the small value of k_z found experimentally in $(Mn_{0.5}In_{0.5})_2MnSbO_6$ (see Figure 2a) are both consistent with this mechanism.

It is very likely that frustration of the Heisenberg symmetric exchange and the antisymmetric interactions imposed by the polar structural distortions are both engaged into formation of the low-temperature modulated ground state. The former mechanism defines the relative magnetic phases of Mn spins between the three symmetry inequivalent sites *M*1, *M*2 and *M*3 (three sublattices) and the latter promotes the slow global spin rotation along the *c*-axis. A possible reason why the modulated state does not develop below the first transition at T_{N1} = 38 K is a partial lifting of the frustration via adopting different magnitudes of the ordered moments for the distinct sublattices. In other words, the system can control the level of the frustration by varying the ordered moments of the sublattices, and fixing them

at certain ratios. This degree of freedom, affecting both symmetric and anti-symmetric exchange, is available only at temperatures close to the transition, where the spins are far from saturation, and it is expected to vanish at lower temperatures. Note, this assumption can explain the magnetisation observed in *M vs H* hysteresis loops and the plateau in the temperature dependence of the ordered moment in the 15 < T < 30 K range (Fig. 3c). However, single crystal neutron diffraction will be needed in order to refine the magnetic moments of the three sublattices independently.

The lock-in transition with the commensurate value k_z = 1/8 implies an activation of the free-energy invariant that selects the commensurate value for the propagation vector[41]. In the case of $(Mn_{0.5}In_{0.5})_2MnSbO_6$, analysis of the allowed free-energy terms revealed that the lock-in invariant indeed exists and it involves the order parameter components in an unprecedented 24th power, $\rho^{24}+\rho^{*24}+\xi^{24}+\xi^{*24}$. Here, ρ,ρ^* and ξ,ξ^* are components of the complex magnetic order parameters of the modulated ground state, describing helices with opposite chirality (see Tables S9 and S10 in the Supplemental Information). This is a remarkably high-power term and to the best of our knowledge, $(Mn_{0.5}In_{0.5})_2MnSbO_6$ is a unique example where lock-in takes place at such a small value of the propagation vector and implies a periodicity of ~114 Å (note that k_2 = [0 0 1/8] in the hexagonal setting of the rhombohedral cell corresponds to k_2 = [1/24 1/24 1/24], in the primitive setting).

IV. CONCLUSIONS

$(Mn_{0.5}In_{0.5})_2MnSbO_6$ OIL polymorph was synthesised under high pressure and high temperature conditions, stabilising a partial Mn/In cation order. This polymorph exhibits a sequence of magnetic phase transitions at 38 K, 17 K and 8 K. The first one gives rise to a commensurate magnetic structure with propagation vector k_1 = [0 0 0], where the Mn^{2+} spins are arranged into honeycomb (*M*1 and *M*3 sites) and triangular (*M*2) sublattices with a net ferromagnetic component. The second transition results in an incommensurately modulated state with k = [0 0 k_z], which locks into the commensurate value k_z = 1/8, below 8 K. The complex magnetic behavior is likely to be associated with magnetic frustration of the symmetric Heisenberg exchange and the polar nature of the crystal structure promoting DM interactions. The role of the anti-symmetric interactions in formation of the modulated ground state of $(Mn_{0.5}In_{0.5})_2MnSbO_6$ is likely to be similar to that in other notable non-centrosymmetric magnets like skyrmion-forming MnSi and multiferroic $BiFeO_3$.

ACKNOWLEDGEMENTS

The authors thank EPSRC, STFC and the Royal Society for support. MINECO and Comunidad de Madrid are also acknowledged for funding through projects MAT2017-84385-R, and S-2013/MIT-1275 respectively. A.M.A.L. thanks a Marie-Słodowska Individual Fellowship in the Horizon 2020 research and innovation programme. We thank ISIS and ALBA-Synchrotron for awarding beam-time in WISH and BL04-MSPD beam-lines respectively. Thanks to Dr. O. Vallcorba for help on SXRD experiments and to L. Huerta Arcos for help on the XPS experiments.

[1] J. A. Rodgers, A. J. Williams, and J. P. Attfield. Z. Naturforsch. **61b**, 1515 (2006).
[2] M. Markkula, A. M. Arevalo-Lopez, A. Kusmartseva, J. A. Rodgers, C. Ritter, H. Wu, and J. P. Attfield. Phys. Rev. B, **84**, 094450 (2011).
[3] A. M. Arevalo-Lopez, and J. P. Attfield. Phys. Rev. B, **88**, 104416 (2013).
[4] S. Vasala, and M. Karppinen. Prog. Solid State Chem. **43**, 1-36 (2015).
[5] G. H. Cai, M. Greenblatt, and M.R. Li. Chem. Matter. **29**, 5447-5457 (2017).
[6] P. S. Wang, W. Ren, L. Bellaiche, and H. J. Xiang. Phys. Rev. Lett. **114**, 147204 (2015).
[7] G. Song, and W. Zhang. Sci. Rep. **6**, 20133 (2016).
[8] R. E. Newnham, and E. P. Meagher. Mat. Res. Bull. **2**, 549 (1967).
[9] S. A. Ivanov, R. Mathieu, P. Nordblad, R. Tellgren, C. Ritter, E. Politova, G. Kaleva, A. Mosunov, S. Stefanovich, and M. Weil. Chem. Mater. **25**, 935−945 (2013).
[10] M. Retuerto, S. Skiadopoulou, F. Borodavka, C. Kadlec, F. Kadlec, J. Prokleška, Z. Deng, J. A. Alonso, M. T. Fernandez-Diaz, F. O. Saouma, J. I. Jang, D. Legut, S. Kamba, and M. Greenblatt. Phys. Rev. B, **97**, 144418 (2018).
[11] E. Solana-Madruga, A. J. Dos santos-García, A. M. Arevalo-Lopez, D. Ávila-Brande, C. Ritter, J. P. Attfield, and R. Sáez-Puche. Dalton Trans. **44**, 20441−20448 (2015).

[12] M. R. Li, E. E. McCabe, P. W. Stephens, M. Croft, L. Collins, S. V. Kalinin, Z. Deng, M. Retuerto, A. S. Gupta, H. Padmanabhan, V. Gopalan, C. P. Grams, J. Hembergher, F. Orlandi, P. Manuel, W.M. Li, C. Q. Jin, D. Walker, and M. Greenblatt. Nat. Comm. **8**, 2037 (2017).
[13] M.-R. Li, M. Croft, P. W. Stephens, M. Ye, D. Vanderbilt, M. Retuerto, Z. Deng, C. P. Grams, J. Hemberger, J. Hadermann, W.-M. Li, C.-Q. Jin, F. O. Saouma, J. I. Jang, H. Akamatsu, V. Gopalan, D. Walker, and M. Greenblatt. Adv. Mater. **27**, 2177−2181 (2015).
[14] M.-R. Li, D. Walker, M. Retuerto, T. Sarkar, J. Hadermann, P. W. Stephens, M. Croft, A. Ignatov, C. P. Grams, J. Hemberger, I. Nowik, P. S. Halasyamani, T. T. Tran, S. Mukherjee, T. S. Dasgupta, and M. Greenblatt. Angew. Chem. Int. Ed. **52**, 8406−8410 (2013).
[15] M.-R. Li, P. W. Stephens, M. Retuerto, T. Sarkar, C. P. Grams, J. Hemberger, M. C. Croft, D. Walker, and M. Greenblatt. J. Am. Chem. Soc. **136**, 8508−8511 (2014).
[16] M.-R. Li, M. Retuerto, D. Walker, T. Sarkar, P. W. Stephens, S. Mukherjee, T. S. Dasgupta, J. P. Hodges, M. Croft, C. P. Grams, J. Hemberger, J. Sánchez-Benítez, A. Huq, F. O. Saouma, J. I. Jang, and M. Greenblatt. Angew. Chem. Int. Ed. **53**, 10774−10778 (2014).
[17] M.-R. Li, M. Retuerto, P. W. Stephens, M. Croft, D. Sheptyakov, V. Pomjakushin, Z. Deng, H. Akamatsu, V. Gopalan, J. Sánchez-Benítez, F. O. Saouma, J. I. Jang, D. Walker, and M. Greenblatt. Angew. Chem. Int. Ed. **55**, 9862−9867 (2016).
[18] Y. S. Oh, S. Artyukhin, J. J. Yang, V. Zapf, J. W. Kim, D. Vanderbilt, and S.-W. Cheong. Nat. Comm. **5**, 3201 (2014).
[19] J. W. Kim, S. Artyukhin, E. D. Mun, M. Jaime, N. Harrison, A. Hansen, J. J. Yang, Y. S. Oh, D. Vanderbilt, V. S. Zapf, and S.-W. Cheong. Phys. Rev. Lett. **115**, 137201 (2015).
[20] A. N. Bogdanov, U. K. Robbler, M. Wolf, and K. H. Muller. Phys. Rev. B. **66**, 214410 (2002).
[21] A. P. Pyatakov, and A. K. Zvezdin. EPL. **107**, 67002 (2014).
[22] U. K. Robler, A. A. Leonov, and A. N. Bogdanov. J. Phys.:Conf. Ser. **303**, 012105 (2011).
[23] I. Sosnowska, and A. K. Zvezdin. J. Magn. Magn. Mater, **167**, 140-144 (1995).
[24] Z. V. Gareeva, A. F. Popkov, S. V. Soloviov, and A. Z. Zvezdin. Phys. Rev. B, **87**, 214413 (2013).
[25] T. Nakajima, H. Oike, A. Kikkawa, E. P. Gilbert, N. Booth, K. Kakurai, Y. Taguchi, Y. Tokura, F. Kagawa, and T. Arima. Sci. Adv., **3**, e1602562 (2017).
[26] T. Zhao, A. Scholl, F. Zavaliche, K. Lee, M. Barry, A. Doran, M. P. Cruz, Y. H. Chu, C. Ederer, N. A. Spaldin, R. R. Das, D. M. Kim, S. H. Baek, C. B. Eom, and R. Ramesh. Nat. Mat. **5**, 823-829 (2006).
[27] J. Rodriguez-Carvajal, Physica B, **192**, 55 (1993).
[28] S. A. Ivanov, P. Nordblad, R. Mathieu, R. Tellgren, E. Politova, and G. André. Eur. J. Inorg. Chem. 4691–4699 (2011).
[29] P. M. Woodward, A. W. Sleight, L. Sh. Du, and C. P. Grey. J. Solid State Chem. **147**, 99-116 (1999).
[30] R. D. Shannon, and C. T. Prewitt, Acta Crystallogr. B, **25**, 925 (1969).
[31] J. P. Attfield, Solid State Sci. **8**, 861–867 (2006).
[32] M. Oku, K. Hirokawa, and S. Ikeda, J. Electron Spectrosc. Relat. Phenom., **7**, 465 (1975).
[33] V. D. Castro, and G. Polzonetti, J. Electron Spectrosc. Relat. Phenom., **48**, 117 (1989).
[34] W. E. Morgan, W. J. Stec, and J. R. Van Wazer, Inorg. Chem., **12**, 953 (1973).
[35] A. Aoki, Jpn. J. Appl. Phys., **15**, 305 (1976).
[36] M. A. Stranick, Surf. Sci. Spectra, **6**, 39 (1999).
[37] R. Hesse, Unifit Line Positions and Data Formats – Version 2019.
[38] J. Cumby, and J. P. Attfield. Nat. Comm. **8**, 14235 (2017).
[39] J. C. Toledano, and P. Toledano, The Landau Theory of Phase Transitions. World Scientific, Singapore, (1987).
[40] Y. A. Izumov, and V. N. Syromyatnikov, Phase Transitions and Crystal Symmetry. Springer, Dordrecht, Netherlands, (2011).
[41] A. Saxena, and G. R. Barsch. Phase Transitions. **46**, 89-142 (1994).
[42] See Supplemental Material at [URL will be inserted by publisher] for further details on the XPS experimental conditions and supporting figures and tables.